Microglial CD11b Knockout Contributes to Axonal Debris Clearance and Axonal Degradation Attenuation via IGF-1 After Acute Optic Nerve Injury

Jiaxing Zhou,[1] Sen Lin,[2] Qiumei Hu,[1] Xue Li,[1] Xi Chen,[1] Linlin Luo,[1] Shiyang Ye,[3] Wei Liu,[1] and Jian Ye[1]

[1]Department of Ophthalmology, Daping Hospital, Army Medical Center of PLA, Third Military Medical University (Army Medical University), Chongqing, China
[2]Department of Neurology, Xinqiao Hospital and The Second Affiliated Hospital, Third Military Medical University (Army Medical University), Chongqing, China
[3]Southwest Hospital/Southwest Eye Hospital, Third Military Medical University (Army Medical University), Chongqing, China

Correspondence: Jian Ye, Department of Ophthalmology, Daping Hospital, Army Medical Center of PLA, Third Military Medical University (Army Medical University), No. 10, Changjiang Branch, Daping, Yuzhong, Chongqing 400042, China; yejian1979@163.com.
Wei Liu, Department of Ophthalmology, Daping Hospital, Army Medical Center of PLA, Third Military Medical University (Army Medical University), No. 10, Changjiang Branch, Daping, Yuzhong, Chongqing 400042, China; wendaowangwei@126.com.
Shiyang Ye, Southwest Hospital/Southwest Eye Hospital, Third Military Medical University (Army Medical University), No. 29, Gaotanyan Main Street, Shapingba, Chongqing 400038, China; yeshiyang1989@foxmail.com.

SY, WL, and JY contributed equally to this work.

Received: November 15, 2022
Accepted: April 6, 2023
Published: May 5, 2023

Citation: Zhou J, Lin S, Hu Q, et al. Microglial CD11b knockout contributes to axonal debris clearance and axonal degradation attenuation via IGF-1 after acute optic nerve injury. *Invest Ophthalmol Vis Sci.* 2023;64(5):7. https://doi.org/10.1167/iovs.64.5.7

Purpose. Microglial clearance of axonal debris is an essential response for management of traumatic optic neuropathy. Inadequate removal of axonal debris leads to increased inflammation and axonal degeneration after traumatic optic neuropathy. The present study investigated the role of CD11b (Itgam) in axonal debris clearance and axonal degeneration.

Methods. Western blot and immunofluorescence were used to detect CD11b expression in the mouse optic nerve crush (ONC) model. Bioinformatics analysis predicted the possible role of CD11b. Cholera toxin subunit B (CTB) and zymosan were used to assay phagocytosis by microglia in vivo and in vitro, respectively. CTB was also used to label functionally intact axons after ONC.

Results. CD11b is abundantly expressed after ONC and participates in phagocytosis. Microglia from *Itgam*$^{-/-}$ mice exhibited more significant phagocytosis of axonal debris than wild-type microglia. In vitro experiments confirmed that the CD11b gene defect in M2 microglia leads to increased insulin-like growth factor-1 secretion and thus promotes phagocytosis. Lastly, following ONC, *Itgam*$^{-/-}$ mice exhibited elevated expression of neurofilament heavy peptide and Tuj1, along with more intact CTB-labeled axons when compared with wild-type mice. Moreover, the inhibition of insulin-like growth factor-1 decreased CTB labeling in *Itgam*$^{-/-}$ mice after injury.

Conclusions. CD11b limits microglial phagocytosis of axonal debris in traumatic optic neuropathy, as demonstrated by increased phagocytosis with CD11b knockout. The inhibition of CD11b activity may be a novel approach to promote central nerve repair.

Keywords: CD11b, IGF-1, microglia, optic nerve injury, phagocytosis

Traumatic optic neuropathy (TON) is a pathological condition in which a massive loss of retinal ganglion cells and their axons is caused by direct or indirect optic nerve injury, resulting in irreversible visual impairment. Cellular debris plays a key role in TON damage. On the one hand, this debris expresses a series of proteins that inhibit axonal regeneration[1,2]; on the other hand, the remaining cellular debris is a mediator of inflammation and induces diffuse axonal injury. Therefore, eliminating myelin and axonal debris can profoundly impact the outlook for TON.

In the central nervous system (CNS), microglia are professional phagocytes. They respond rapidly to tissue damage by

Copyright 2023 The Authors

This work is licensed under a Creative Commons Attribution-NonCommercial-NoDerivatives 4.0 International License.

proliferating, migrating, and removing debris.[3,4] In response to injury, microglia are quickly activated. However, in CNS injury, microglia exhibit a low capacity for phagocytosis, resulting in axonal and myelin debris residing in the tissue for months.[5]

Microglia recognize dead cells and cell debris through multiple surface receptors and subsequently activate downstream signaling pathways for phagocytosis.[6–8] It is well-established that clearance of axonal and myelin debris after CNS injury involves the activation of complement signaling cascades.[6,9] CD11b is encoded by the *Itgam* gene. It is a component of complement receptor 3, a critical surface receptor in the complement signaling pathway that regulates microglial phagocytosis of cellular debris.[10] Our previous study[11] indicates that CD11b is abundantly expressed after injury. However, despite these important findings, the role of CD11b in microglial phagocytosis still requires further investigation.

In the present study, we investigate the differences in phagocytic activity of microglia between CD11b knockout mice (*Itgam*$^{-/-}$) and C57BL/6J wild-type (WT) mice using the ONC model and reveal the possible molecular mechanisms involved.

Methods

Animals and Genotyping

All animal procedures were carried out following the guidelines of the Institutional Animal Care and Use Committee of the Army Medical University, Chongqing, China, and handled according to the ARVO Statement for the Use of Animals in Ophthalmic and Vision Research.

Adult C57BL/6J mice (male, aged 6–8 weeks; weight, 20–24 g) were purchased from the Animal Center of Army Medical University. B6.129S4-*Itgam*^{tm1Myd}/J mice (JAX, Cat. No. 003991) were purchased from Jackson Laboratory (Bar Harbor, ME, USA). The genotyping identification is shown in Supplementary Figure S1A. The primer sequences used are shown in Table 1. Western blot (WB) tests confirmed CD11b knockout in *Itgam*$^{-/-}$ mice (Supplementary Fig. S1B). All animals were housed and maintained in a specific pathogen-free facility under a 12/12 h light–dark cycle, with ad libitum access to food and water.

Bioinformatics Analysis of CD11b-Associated Genes

To investigate the changes of CD11b-associated genes at day 7 after ONC, we searched the Retrieval Interacting Genes (STRING) 11.5 database (http://string-db.org/),[12] using a single protein name (Itgam) and an organism (*Mus musculus*). The main parameters were set as follows: minimum required interaction score (medium confidence of 0.400), the meaning of network edge meaning (evidence line color indicates the type of interaction evidence), and Max number of Interactors to show the maximum number of interactors (no more than 250 interactors).

Table 1. Primer Sequences Used for Genotyping Identification

Primer Description	Primer Sequences (5′–3′)
Mutant forward	ATCGCCTTCTTGACGAGTTC
WT forward	CATACCTGTGACCAGAAGAGC
Common reverse	TAGGCTATCCAGAGGTAGAC

Screening of Differentially Expressed Genes (DEGs) at Day 7 After ONC

The gene expression dataset GSE40857[13] was acquired by the Gene Expression Omnibus (GEO)[14] databases. The GSE40857 dataset used microarray to identify differentially expressed genes in mice from 1 day to 3 weeks after ONC. We applied GEO2R[15] to detect the DEGs between naïve control and samples after 7 days after injury in GSE40857. The results are presented in a table of genes ordered by significance. We considered DEGs as | log2 (fold change) | $\geq$ 1.8 and a P value of <0.01.

Gene Enrichment Analysis

Venn diagrams were performed by the website jvenn.[16] Heatmaps were generated by the pheatmap R package (version1.0.12.). On the common genes from the two datasets, Gene Ontology (GO)[17] and Tissue expression (TISSUES)[18] were performed using STRING 11.5. A false discovery rate of <0.05 was identified as a significant difference. The ggplot2 R package (version 3.3.5)[19] was used for visualization.

Optic Nerve Crush (ONC) Model

Mice were intraperitoneally injected with 1% pentobarbital sodium for anesthesia. The classic model of ONC was performed as previously described.[20,21] The exposed optic nerve of the left eye was crushed for 5 seconds at 1.5 mm behind the eyeball with ultrafine self-closing forceps without damage to the retinal vessels or the blood supply. The right eye was used as a control. All procedures were performed aseptically, and no postoperative infections were observed.

Intravitreal Injections

After anesthesia, mice received intravitreal injections of cholera toxin subunit B (CTB) conjugated to Alexa Fluor 647 (Invitrogen, C-34778) dye or Alexa Fluor 555 (Invitrogen, C-34776) dye in their eyes (1 µL per eye at a concentration of 1 µg/µL in sterile PBS). For microglial phagocytic observation, CTB was injected 48 hours before ONC. For axon number observation, CTB was performed 24 hours before mouse sacrifice. The intravitreal injection procedure was performed as described previously.[22]

Primary Microglial Cell Culture

Mixed glial cultures were isolated from the cerebral cortices of 1-day-old C57BL/6 or *Itgam*$^{-/-}$ mice as previously described.[23] The purity of the microglia was confirmed by immunostaining using anti-Iba1 (1:400, rabbit monoclonal, Wako, 019-19741).

Drug Treatment

For the in vivo experiments, LA1(MCE, HY-15701) and AXL1717 (TagerMol, T6943) are permeable to the

Investigative Ophthalmology & Visual Science

Investigative Ophthalmology & Visual Science

blood–brain barrier.[24,25] Mice received intraperitoneal injections of LA1 (1 mg/kg, i.p., twice daily), AXL1717 (40 mg/kg, i.p., twice daily), or solvent-only from 2 hours before surgery until sacrifice. For the in vitro experiments, primary microglial cells were treated with vehicle (cell culture medium), insulin-like growth factor-1 (IGF-1) (100 ng/mL, Bioworld, BK0085), IL-4 (20 ng/mL, MCE, HY-P7080), lipopolysaccharide (LPS) (100 ng/mL, Solarbio, L8880), IL-4 + IGF-1 or LPS + IGF-1 for 24 hours. In some experiments, anti-IGF-1 (1 µg/mL, Abcam, Cambridge, UK; ab9572) or isotype control antibodies were added 2 hours before the end of stimulation.

Immunofluorescence

The optic nerves were dissected after perfusion fixation and immersion-fixed in 4% paraformaldehyde overnight at 4°C. Next, these tissues were dehydrated in 30% sucrose in PBS until cryo-sectioned at a thickness of 12 µm. For most in vivo experiments, three sections of each optic nerve were selected randomly for immunostaining. For microglial engulfment analysis in vivo, a section at the longest transverse diameter of each optic nerve was selected for immunostaining. Fixation of cells was performed by 4% paraformaldehyde at room temperature for 15 minutes. Tissue cryosections and fixed primary microglia were incubated with 0.1% Triton X-100 in PBS at room temperature for 15 minutes, then incubated with primary antibodies at 4°C overnight. Appropriate fluorescent secondary antibodies (Molecular Probes, Eugene, OR, USA) were applied for 1 hour at room temperature. The slides were mounted after nuclei counterstaining (DAPI). Images were captured at a fixed area by an Olympus confocal microscope. For most sections, images of the optic nerve stump were captured centered on the crush site or bounded by the proximal edge of the crush site, and the tissue area was analyzed for mean pixel intensity or colocalization coefficient of two channels using Fiji software (National Institutes of Health, Bethesda, MD, USA) as previously described,[26–28] then averaged with two to three sections from one nerve as the data for this nerve. For microglial engulfment analysis in vivo, z-step images (0.5 µm, 12 sections per z-step) of the optic nerve stump were captured at a 200-µm distance from the proximal edge of the crush site at 60 × magnification to exclude interference from the glial scar. Microglia engulfing axonal debris ($Iba1^+$ areas containing CTB^+ points) were counted in z-step images using Fiji software, and each microglia was counted only once. Then, in each z-step image, the size of these microglia and the size of their engulfed axonal debris were measured individually by Fuji software and separately multiplied by 0.5 µm, and the data from 12 z-step images of one optic nerve were summed as the total volume of this microglia and the volume of its engulfed axonal debris. To determine percentage engulfment the following calculation was used: (volume of internalized debris)/(volume of microglial cell) × 100.[10]

The primary antibodies used in this work are anti-Iba1(Novus, NB100-1028), anti-CD11b (Bio-Rad, Hercules, CA, USA; MCA711), anti-CD68 (Bio-Rad, MCA1957), CD206 (Cell Signaling Technology, Danvers, MA, USA; 24595), anti–IGF-1 (Abcam, ab9572), anti-Arginase 1 (ABclonal Science, Inc, Woburn, MA, USA; A4923), and anti-16/32 (Novis Biologicals, Centennial, CO, USA, NBP2-52644).

Immunohistochemistry

Cryosections of the optic nerve were performed using the same methods as for immunofluorescence. Then fixed sections were treated with 0.1% Triton X-100 and 0.6% hydrogen peroxide. Immunohistochemical staining was performed according to the standard procedure of the SP-POD Kit (Solarbio Life Science, Beijing, China; SP0021) instructions. The primary antibody used in this work is anti–neurofilament heavy peptide (NF-H) (Abcam, ab40796). Three sections of each optic nerve were randomly selected for immunostaining. The image of the proximal segment of the optic nerve at the edge of the injured site was captured by an Olympus optical microscope. The $NF\text{-}H^+$ area and the tissue area were measured by Fiji software at a fixed threshold. The results of the three sections were averaged to obtain the $NF\text{-}H^+$ area and the tissue area for each optic nerve. The percentage of $NF\text{-}H^+$ area was determined by the following formula: (the $NF\text{–}H^+$ area)/(the tissue area) × 100.

Immunoblotting

WB analysis was performed on proteins extracted from freshly dissected tissue samples (optic nerve, retina, cerebellum, lung, and spleen) as previously described.[11] The optic nerve was only taken from a segment approximately 3-mm long centered on the crush site. Washed and blocked polyvinylidene fluoride membranes from WBs were incubated with primary antibodies. Primary antibodies included anti-CD11b (Abcam, ab133357), anti–IGF-1 (ABclonal, A11985), anti–p-S6 (ABclonal, AP0502), anti–NF-H (Abcam, ab40796), anti–Tuj1 (Abcam, ab18207), and anti–β-actin (Bioworld, New York, NY, USA; BS6007). At room temperature, appropriate horseradish peroxidase-conjugated secondary antibodies (Santa Cruz Biotechnology, Dallas, TX, USA) were applied for 1.5 hours. ECL-Plus reagent (Biogrund, Shelbyville, KY, USA) was applied to the membranes, and chemiluminescence was visualized by an Odyssey Fc Imaging System (Licor, Lincoln, NE, USA). Quantification of immunoreactive bands was reported as a gray value ratio against β-actin using Fiji software.

ELISA

The level of IGF-1 in the medium of microglia was quantified by ELISA with mouse IGF-1 (ABclonal, Woburn, MA, USA; RK00171) following the manufacturer's protocols. The absorbance was detected at 450 nm using a microplate reader (Biotek, Winooski, VT, USA). The concentration of IGF-1 was calculated according to the absorbance value and the standard curve. Each group of cells was seeded at the same density. Experiments were carried out three independent times, with sets of three technical repeat wells per experiment. The mean values obtained in each experiment were used for statistical analysis.

Microglial Phagocytosis Assay

A phagocytosis assay kit (Abcam, ab234053) was used to examine microglial phagocytosis according to the company protocol with minor modifications. Subsequently, the cells were labeled with anti-Iba1. Three to four random visual fields per well were photographed by an Olympus confocal microscope. The average of these fields was used as the data for this well. Quantification of zymosan particles

Table 2. Primer Sequences Used for RT-qPCR

Gene	Forward (5′–3′)	Reverse (5′–3′)
TNF-α	CCTCTTCTCATTCCTGCTTG	TCTGGGCCATAGAACTGATG
CD86	ACTTACGGAAGCACCCACG	CTTTGTAAATGGGCACGGC
IL-1β	ACGGACCCCAAAAGATGAAG	AGGCCACAGGTATTTTGTCG
IL-6	ATACCACTCCCAACAGACC	TGCATCATCGTTGTTCATAC
CD206	CCACGGATGACCTGTGCTC	GGTTCCACACCAGAGCCATC
Arg-1	CAACACTCCCCTGACAACC	ACGATGTCTTTGGCAGATATG
IL-10	AGCCGGGAAGACAATAACTG	GGAGTCGGTTAGCAGTATGTTG
IGF-1	CACATCATGTCGTCTTCACACC	GGAAGCAACACTCATCCACAATG

phagocytosed by microglia was shown as the total number of zymosan particles within the Iba1$^+$ area/the number of Iba1$^+$ cells in each visual field. Zymosan particles and Iba1-positive cells were counted using Fiji software. The experiment was repeated three times independently, each time with two to three wells per group. Data from three independent experiments were quantified.

RT-qPCR

Total RNA was extracted from a segment of the optic nerve approximately 3-mm long centered on the crush site using the RNeasy RNA Isolation Kit (Qiagen, Hilden, Germany) according to the manufacturer's protocol. Reverse transcription reactions were performed using the PrimeScript RT reagent Kit (Takara Bio, Inc, Shiga, Japan). RT-qPCR was performed in a CFX96 real-time instrument C1000 Thermal Cycler (Bio-Rad) using the SYBR method (Quanta BioSciences, Beverly, MA, USA). The results were normalized to β-actin. Relative quantification was calculated using the $2-\Delta\Delta Cq$ method. All reactions were performed in duplicate for at least three independent runs. The Primer sequences used for qRT-PCR in this study are listed in Table 2.

Statistical Analysis

Statistical analyses were performed using GraphPad Prism 7.0 software (GraphPad, La Jolla, CA, USA) and reported as mean ± SEM. The Student t test, one-way ANOVA, and least significant difference post hoc tests were used. Each group in all experiments contains at least three biological replicates ($n \geq 3$). All experiments were performed independently more than three times. P values of ≤ 0.05 were considered statistically significant. Significant values were marked as * ($P < 0.05$), ** ($P < 0.01$), and *** ($P < 0.001$).

Results

CD11b Is Upregulated Around the Crush Site After ONC

To investigate the role of CD11b in optic nerve injury, we first examined the protein expression levels of CD11b around the crush site in a mouse ONC model. The WB results (Figs. 1A and B) suggest CD11b was significantly elevated on day 5 after injury, peaked on day 7, and

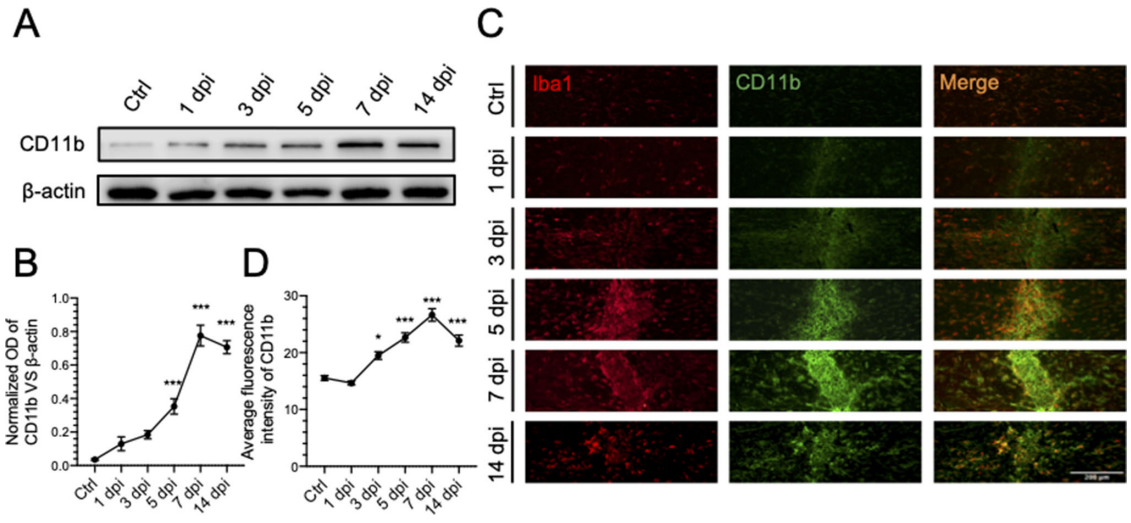

Figure 1. Detection of CD11b protein expression in optic nerve by WB and IF. (**A**) WB showing the expression levels of CD11b in intact (control), 1 dpi, 3 dpi, 5dpi, 7 dpi, and 14 dpi optic nerve. β-Actin was used as a loading control. (**B**) Quantitative analysis indicates that the expression of CD11b protein in the WT optic nerve was very low in the resting state but significantly increased after ONC and maintained at a high level until at least 14 dpi. The data shows the mean value of the gray value ratio from three independent experiments (mean ± SEM, $n = 3$ mice per group). (**C**) Representative images showing immunostaining of CD11b (green) and Iba1 (red) around crush site at 0 dpi (control), 1 dpi, 3 dpi, 5 dpi, 7 dpi, and 14 dpi. Scale bar, 200 µm. (**D**) The average fluorescence intensity of CD11b$^+$ area quantified from three independent experiments (mean ± SEM, $n = 3$ mice per group), related to (**C**). CD11b staining results showed approximately the same trend as WB.

Investigative Ophthalmology & Visual Science

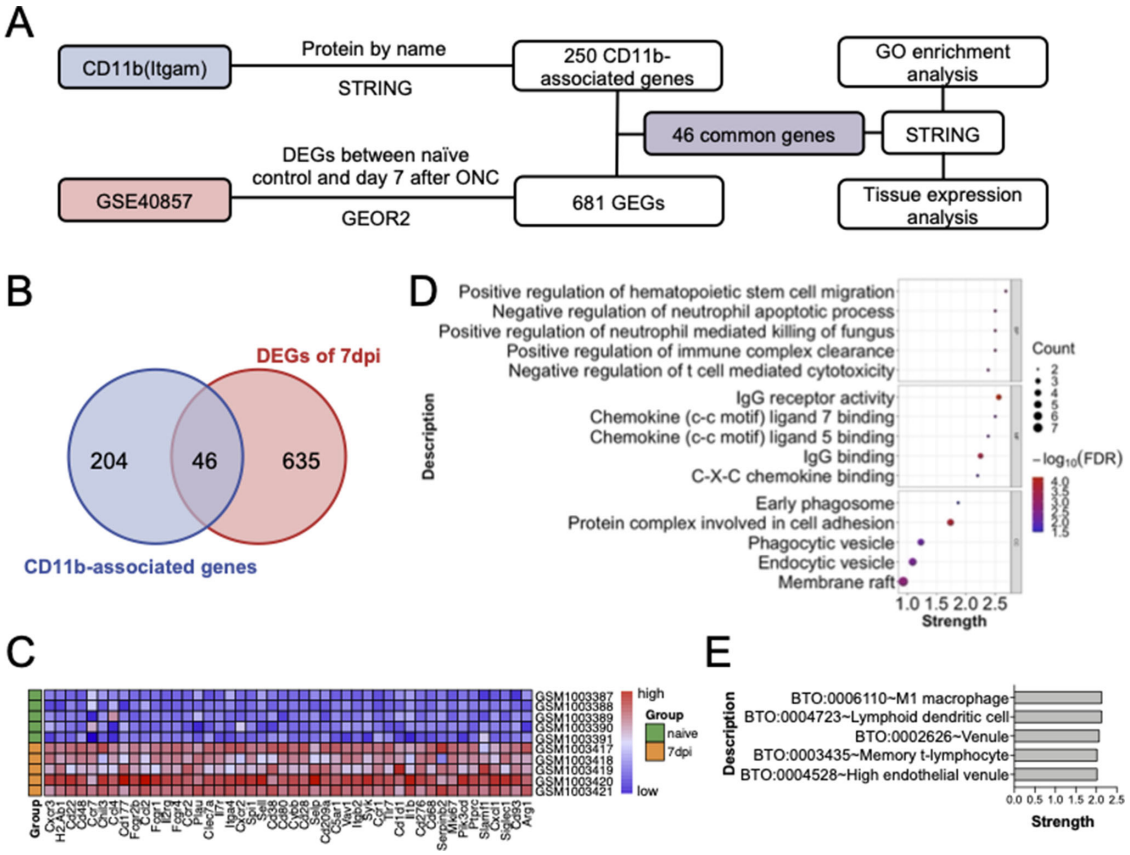

Figure 2. Enrichment analysis of CD11b-associated genes on day 7 after injury. (**A**) The flowchart of Bioinformatics analysis of CD11b-associated genes on day 7 after injury. (**B**) Venn diagram showing common genes from CD11b-associated genes and DEGs of day 7 after injury. We identified 46 genes as common genes. (**C**) Heatmaps of 46 common genes identified in CD11b-associated genes and DEGs of day 7 after injury. Genes upregulated are in *red*. Genes downregulated are in *blue*. Genes without any significant difference are in *white*. The difference was set as | log2 (Fold change) | $\geq$ 1.8 and $P < 0.01$. (**D**) Results of GO enrichment analysis of common genes. STRING mainly uses strength and false discovery rate (FDR) to describe the enrichment effect. Strength is Log10(observed/expected). This measure describes how large the enrichment effect is. The larger the value of strength is, the larger the enrichment effect is. FDR describes how significant the enrichment is. The abscissa represents strength, and the ordinate represents enriched GO. BP represents GO biological process. MF represents GO molecular function. BP represents GO cellular composition. The dot size represents the number and ratio of common genes. Different colors stand for variations of FDR. (**E**) Results of TISSUES analysis of common DEGs. The abscissa represents strength, and the ordinate represents enriched TISSUES.

remained at a high level on day 14. We further examined the distribution and localization of CD11b. Immunofluorescence (IF) results (Figs. 1C and D) show that CD11b colocalized with the microglia marker Iba1 and that CD11b is barely detectable in the absence of injury. CD11b-positive microglia aggregate around the injury site after injury and constitute glial cell scarring. These results are consistent with our previous study in the retina,[11] suggesting that CD11b of microglia is involved in glial scar formation in ONC.

Bioinformatics Analysis of CD11b-Associated Genes on Day 7 After Injury Reveals Phagocytosis Potential

To further explore the critical functions of CD11b after ONC, we analyzed the enrichment of CD11b-associated genes on day 7 after injury by GO enrichment analysis and TISSUES analysis (Fig. 2A). We first used the STRING database to screen 250 genes that may interact with CD11b. Next, we analyzed the data related to day 7 after injury from the dataset GSE40857 by the GEOR2 and obtained a total of 681 DEGs (| log2 FC| $\geq$ 1.8 and $P < 0.01$). A total of 46 common genes were coexpressed in the two datasets (Fig. 2B). The expression of these genes was all elevated on day 7 after ONC (Fig. 2C). We further performed GO enrichment analysis of these genes by the STRING. We show the top five outputs in GO biological process, molecular function, and cell composition, respectively, according to strength (Fig. 2D). In the biological process, Ccr2 and Ccl2 are enriched in the term GO:0090265–positive regulation of immune complex clearance by monocytes and macrophages. In the cellular component, Sky and Tlr7 are enriched in the term GO:0032009–early phagosome. Sky, Tlr7, Cybb, and Slamf1 are enriched in the entry GO:0045335–phagocytic vesicle. We also performed TISSUES analysis using the STRING and show the top five terms with Strength in Figure 2E. In TISSUES analysis, the top ranking is the term BTO: 0006110 – M1 macrophage. Arg1, IL-1b, Ccl2,

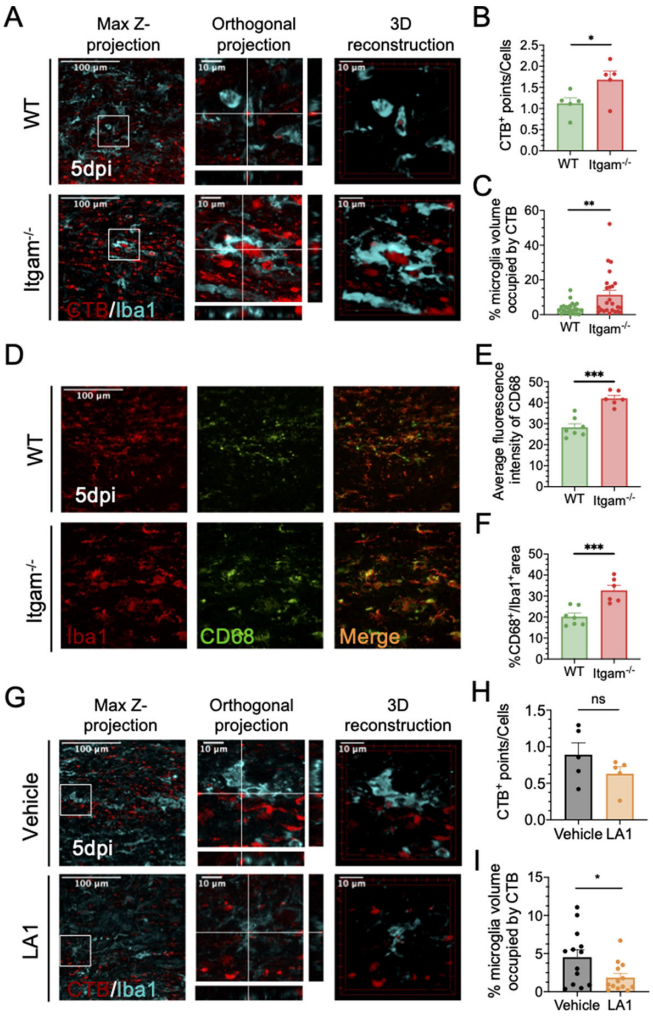

Figure 3. Effect of CD11b on microglial phagocytosis in the optic nerve after ONC. (**A**) Representative images of Z projections, orthogonal slices, and three-dimensional reconstructions of the proximal optic nerve region in WT and *Itgam*$^{-/-}$ mice at 200 µm from the crush site at day 5 after injury, scale bar, 100 µm (enlarged, 10 µm). (**B**) The average number of CTB^{+} points engulfed by microglia in (**A**). Each dot represents the average number of one mouse (mean ± SEM, $n = 5$ mice per group). (**C**) Quantification of the percentage engulfment (volume of internalized debris/volume of microglial cell × 100) in (**A**). Each dot represents the percentage engulfment of one microglia in (**A**) (mean ± SEM, $n = 5$ mice per group). (**D**) Representative images show immunofluorescent staining of CD68 (*green*) and Iba1 (*red*) in the optic nerve at day 5 after injury. Scale bar, 100 µm. (**E**, **F**) Quantitative analysis illustrating that both the average CD68 fluorescence intensity and the percentage of CD68^{+} to Iba^{+} area was significantly higher in *Itgam*$^{-/-}$ mice (mean ± SEM, $n =$ 6–7 mice per group). (**G**) Representative images of Z-projections, orthogonal sections, and three-dimensional reconstructions of WT mice treated with solvent and LA1 at 200 µm from the crush site at day 5 after injury. Scale bar, 100 µm (original magnification, 10 µm). (**H**) The average number of CTB^{+} points engulfed by microglia in (**G**). Each dot represented the average number of one mouse (mean ± SEM, $n = 5$ mice per group). (**I**) Quantification of the percentage engulfment (volume of internalized debris /volume of microglial cell × 100) in (**G**). Each dot represented the percentage engulfment of one microglia in G (mean ± SEM, $n = 3$ mice per group).

and Chil3 are enriched in this term. Our results suggest the possibility that CD11b regulates cellular phagocytosis in ONC and may be involved in microglia/macrophage polarization.

CD11b Knockout Significantly Enhances Microglial Phagocytosis Around the Crush Site

Microglia are the major phagocytic cells in the CNS. Because CD11b was upregulated after optic nerve injury and bioinformatics analysis predicted its possible role in the regulation of phagocytosis in ONC, we next addressed whether CD11b regulates the microglial phagocytosis following ONC using *Itgam*$^{-/-}$ mice. We prelabeled the axons of retinal ganglion cells using Alexa FL 555 CTB conjugate (CTB-555). At day 7 after injury, we did not observe significant colocalization of CTB-555 and microglial marker Iba1 in either WT or *Itgam*$^{-/-}$ mice (data not shown). Considering that the microglial phagocytosis may occur early in the injury, we then examined the phagocytosis by microglia on day 5 after the injury.[29] In the optic nerve of WT and *Itgam*$^{-/-}$ mice, we observed CTB-555 labeled axonal debris within microglia, indicating microglial phagocytosis of the axonal debris (Fig. 3A). The measurements of the number[30] and area/volume[10,31] of engulfed particles are common methods to evaluate the phagocytic capacity of cells. In our experiments, the average number of CTB^{+} axon debris phagocytosed by microglia in *Itgam*$^{-/-}$ mice was significantly higher than in WT (Figs. 3A and B). By further measurement of axon debris volume (presented as the percentage of microglial volume), we found that the volume of axon debris in microglia was also significantly higher in *Itgam*$^{-/-}$ mice (Figs. 3A and C). These results suggest that CD11b knockdown enhanced the phagocytosis of axon debris by microglia. Because CD68 is a marker of lysosomes[32] and the size of its area is positively correlated with phagocytic activity,[29] we detected the expression of CD68 after injury by IF. As shown in Figure 3D, in *Itgam*$^{-/-}$ mice, most CD68^{+}Iba1^{+} microglia exhibited a large and rounded morphology with fewer branches, showing high phagocytic activity. The fluorescence intensity and area of CD68^{+} points were also elevated in *Itgam*$^{-/-}$ mice (Figs. 3E and F).

To further confirm the modulation of phagocytosis by CD11b, we used LA1, a CD11b-specific agonist, to activate CD11b in WT mice. At day 5 after injury, LA1 treatment did not alter the number of CTB^{+} points phagocytosed by microglia compared with solvent-treated WT mice (Figs. 3G and H). However, LA1 significantly decreased the volume occupied by CTB^{+} points in microglia, suggesting diminished microglial phagocytosis in the LA1 group (Figs. 3G and I). In sum, our findings demonstrate that CD11b knockout promoted phagocytosis of axonal debris by microglia around the crush site in ONC.

The Expression of IGF-1 Is Markedly Elevated in *Itgam*$^{-/-}$ Mice After ONC

Next, we sought to explore the potential causes for the enhanced microglial phagocytosis under CD11b knockout conditions. Considering that CD11b-related genes in ONC may be involved in microglia and macrophage polarization (Fig. 2E). We tested the mRNA levels of M1 and M2 type markers in the optic nerve at day 5 after injury by qPCR. The markedly elevated IGF-1 mRNA in *Itgam*$^{-/-}$ mice attracted our attention. However, no changes in other factors were detected (Fig. 4A). For further confirmation, we measured the protein level of IGF-1 in the optic nerve

Investigative Ophthalmology & Visual Science

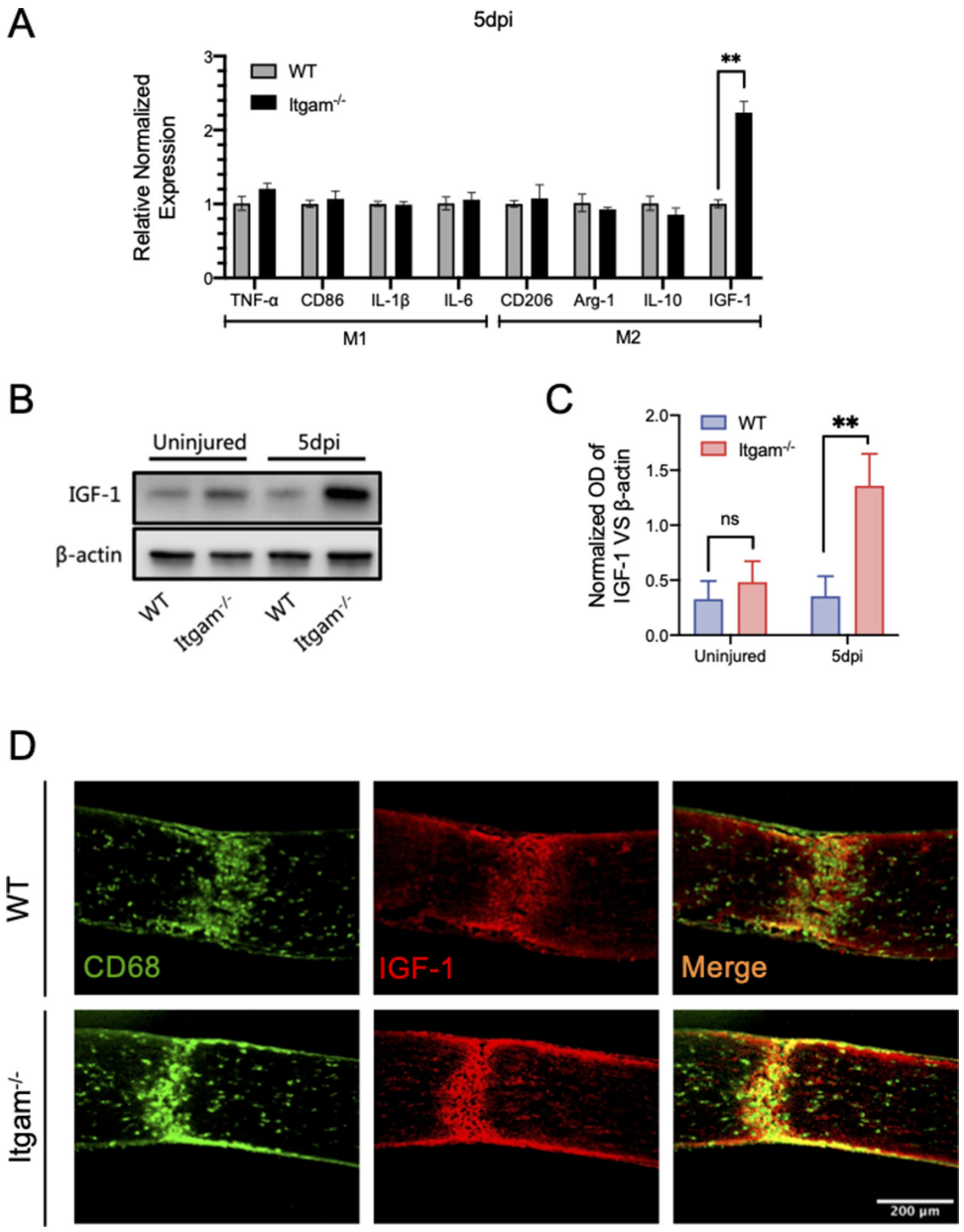

Figure 4. Increased IGF-1 in *Itgam*$^{-/-}$ mice at day 5 after injury. (**A**) The mRNA expression of cytokines in the optic nerve at day 5 after injury was measured by RT-qPCR. Gene expressions were normalized to β-actin. The results represent three independent experiments and are shown as mean ± SEM ($n = 3$ mice per group). (**B**, **C**) WB and quantitative analysis showing expression of IGF-1 in the optic nerve at day 5 after injury. β-Actin was used as a loading control. Quantitative analysis exhibited the mean value of the gray value ratio from three independent experiments (mean ± SEM, $n = 3$ mice per group). (**D**) Representative images showing immunofluorescent staining of CD68 (*green*) and IGF-1 (*red*) in the optic nerve of WT and *Itgam*$^{-/-}$ mice at day 5 after injury. Scale bar, 100 µm.

by WB. IGF-1 was upregulated in *Itgam*$^{-/-}$ mice (Figs. 4B and C). Meanwhile, we used IF to localize the source of IGF-1. We labeled microglia and macrophages using CD68. As shown in Figure 4D, IGF-1^{+} spots were mainly detected in or around CD68^{+} cells in both groups, and IGF-1 signals were enhanced in the *Itgam*$^{-/-}$ group, suggesting that the upregulated IGF-1 in *Itgam*$^{-/-}$ mice mainly originated from microglia/macrophage. Our findings indicate that CD11b knockout promotes microglia- and macrophage-derived IGF-1 expression without altering cell polarization.

Microglial CD11b Knockout Promotes Phagocytosis of M2-Type Microglia Through Upregulating IGF-1

IGF-1 has been reported to be involved in the phagocytosis of a variety of cells.[33,34] Does IGF-1 promote microglial phagocytosis? IGF-1 is a secreted protein. We first measured IGF-1 levels in culture supernatants of WT and CD11b knockout primary microglia in different activation states using ELISA. We chose LPS and IL-4 to induce classical activation (M1) microglia or alternate activation (M2)

Investigative Ophthalmology & Visual Science

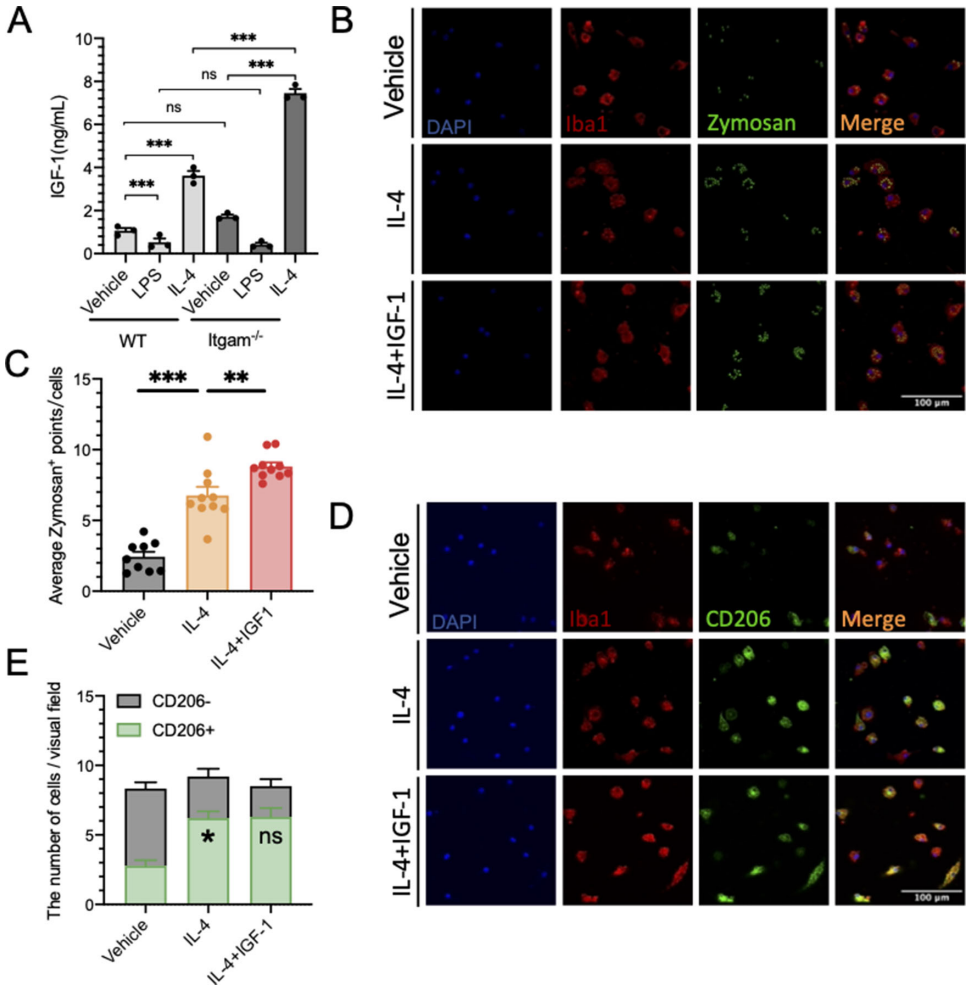

Figure 5. Increased phagocytosis of zymosan by M2-type microglia with IGF-1 when CD11b is deleted. (**A**) Quantification of IGF-1 in WT and *Itgam*$^{-/-}$ primary microglia culture supernatants under different activation states. The level of IGF-1 in the media of microglia was detected by ELISA after 24 hours of treatment with solvent (medium), LPS (100 ng/mL), or IL-4 (20 ng/mL). Data are presented as the mean values of three independent experiments (mean ± SEM, $n = 3$ wells per group). (**B**) Representative images showing immunofluorescent staining of Iba1 (*red*) and zymosan (*green*) with Hoechst (*blue*) nuclear staining in primary *Itgam*$^{-/-}$ microglia after IL-4 and IGF-1 treatment. Scale bar, 100 µm. (**C**) Quantification of the average number of zymosan particles engulfed by microglia in (**B**). Each dot represents the average value of three to four visual fields in one culture (mean ± SEM, $n = 9$–10 wells per group). The quantitative analysis illustrates that IGF-1 promotes phagocytosis of zymosan particles by IL-4–induced M2-type microglia when CD11b is deleted. (**D**, **E**) Representative images and quantitative analysis showing immunofluorescent staining of Iba1 (*red*) and CD206 (*green*) with Hoechst (*blue*) nuclear staining in primary *Itgam*$^{-/-}$ microglia after IL-4 and IGF-1 treatment. Scale bar, 100 µm. The quantitative analysis shows that IL-4 treatment increased the number of CD206^{+}/Iba1^{+} cells, but IL-4 combined with IGF-1 treatment did not vary the number of CD206^{+}/Iba1^{+} cells compared with IL-4 treatment alone. Three to four random visual fields per well were photographed. The average number of cells of these fields was used as the data for this well (mean ± SEM, $n = 9$–10 wells per group, *$P < 0.05$; ns, nonsignificant, compared with the vehicle group).

microglia, respectively.[35] As shown in Figure 5A, IL-4 treatment enhanced IGF-1 secretion and LPS treatment decreased IGF-1 secretion from primary microglia, consistent with the study of Li et al.[36] Under solvent-only treatment, IGF-1 secretion by CD11b knockout primary microglia was not significantly different from that of WT ($P = 0.091$). However, CD11b knockout caused a significant increase in IGF-1 secretion by M2-type microglia. So, does IGF-1 promote phagocytosis in M2 microglia? We examined the phagocytic activity of WT and *Itgam*$^{-/-}$ microglia using prelabeled zymosan particles (Supplementary Fig. S2A). Consistent with previous studies,[37] CD11b knockout resulted in decreased phagocytosis in solvent-treated microglia. Interestingly, the M2 microglial phagocytosis was enhanced by CD11b knockout compared with WT. These findings suggest that the enhanced phagocytosis of *Itgam*$^{-/-}$ microglia may arise from the phagocytosis-promoting effect of IGF-1 on M2-type microglia. To verify this hypothesis, we stimulated IL-4–treated CD11b knockout microglia using exogenous IGF-1. In our experiments, *Itgam*$^{-/-}$ microglia under IL-4 stimulation phagocytosed zymosan particles approximately three times more than the vehicle. At the same time, IL-4 combined with IGF-1 treatment caused *Itgam*$^{-/-}$ microglia to exhibit stronger phagocytosis, which was about four times higher than the vehicle and statistically significantly different from the IL-4 group (Figs. 5B and C). However, we did not observe the promotion of phagocytosis by IGF-1 in resting or LPS-induced M1-type microglia (Supplementary Fig. S3A and B). To exclude the possibility that IGF-1 is enhancing phagocytosis by inducing *Itgam*$^{-/-}$ microglia conversion to an M2 type, we used CD206 to label M2-type microglia. As Figures 5D and E show, IL-4 combined with IGF-1 treat-

Investigative Ophthalmology & Visual Science

ment did not vary the number of $CD206^+/Iba1^+$ cells compared with IL-4 treatment alone. Our results show that CD11b knockout promotes phagocytosis of M2-type microglia through up-regulating IGF-1 without affecting the polarization of microglia.

Blocking IGF-1 Signaling Impairs the Phagocytosis by M2-Type Microglia When CD11b Is Deleted

Next, we used neutralizing antibodies to inhibit IGF-1 activity in IL-4–treated *Itgam*$^{-/-}$ microglia. Here we used rabbit IgG as an isotype control antibody and IgG treatment did not alter IGF-1 secretion from *Itgam*$^{-/-}$ microglia (Supplementary Fig. S4A). As shown in Figures 6A and B, the number of zymosan particles phagocytosed by *Itgam*$^{-/-}$ microglia in the IL-4 + anti–IGF-1–treated group was significantly lower than in the IL4 + isotype control group and not significantly different from the isotype control group ($P = 0.218$). These results suggest that IGF-1 neutralizing antibodies block IL-4–promoted *Itgam*$^{-/-}$ microglial phagocytosis. In contrast, IGF-1–neutralizing antibodies did not affect the phagocytosis by M1-type microglia when CD11b is deleted (Supplementary Fig. S4B and C). Our findings further demonstrate the critical role of IGF-1 for M2 microglial phagocytosis in *Itgam*$^{-/-}$ microglia.

CD11b/IGF-1 Favors Axonal Stabilization After ONC

Current studies suggest that IGF-1 contributes to the maintenance of axonal stability.[38,39] Together with our experiments, we hypothesize that CD11b knockout enhances axonal stability after injury. To demonstrate this, we measured the protein levels of the axonal markers NF-H and neuronal class III β-Tubulin (Tuj1) in the optic nerve on day 7 after ONC. Consistent with our assumption, WB results (Fig. 7A) showed that *Itgam*$^{-/-}$ mice had higher NF-H (Fig. 7B) and Tuj1 (Fig. 7C) expression than WT mice. CTB transport in nerve fibers requires intact axonal function.[40] Considering that the WB detection of NF-H and Tuj1 may be derived from axonal debris, we labeled functional axons by Alexa FL 647 CTB conjugate (CTB-647) on day 6 after injury. Also, we used AXL1717, an IGF1R inhibitor, to assess the effect of IGF-1 on axonal stability (Fig. 7D). We found that *Itgam*$^{-/-}$ mice had larger fluorescence area than WT mice (Figs. 7E and F). The CTB^+ area in the optic nerve of *Itgam*$^{-/-}$ mice was significantly decreased after the use of AXL1717 compared with solvent control. In contrast, we did not observe a similar phenomenon in WT mice (Figs. 7E and F). It suggests that the effect of decreasing axonal degradation in CD11b knockout mice depends on IGF-1. We also performed immunohistochemical staining on the optic nerve samples. Immunohistochemistry of NF-H showed that *Itgam*$^{-/-}$ mice had a more intact axon morphology (Supplementary Fig. S5A) and a larger area of $NF\text{-}H^+$ (Supplementary Fig. S5B) after ONC than WT mice. AXL1717 treatment blocked this effect in *Itgam*$^{-/-}$ mice (Supplementary Fig. S5A and B), consistent with these results (Figs. 7E and F). These results suggest an important role of IGF-1 in maintaining axonal stability after optic nerve injury in *Itgam*$^{-/-}$ mice.

To further exclude the interference of residual axonal debris, we used CTB-555 and CTB-647 to label all axons before surgery and intact axons after ONC, respectively (Fig. 7G). As shown in Figures 7H, I, and J, the area of CTB-555 colocalized with CTB-647 accounted for 39% of the total CTB555 area in WT mice at day 7 after injury. Yet, this ratio was 62% in *Itgam*$^{-/-}$ mice, significantly higher than in WT mice. Combined with the results in Figure 7E, we proved that the increase of CTB^+ areas in *Itgam*$^{-/-}$ mice were due to the decrease of axon degradation after injury rather than the increase of residual axon debris.

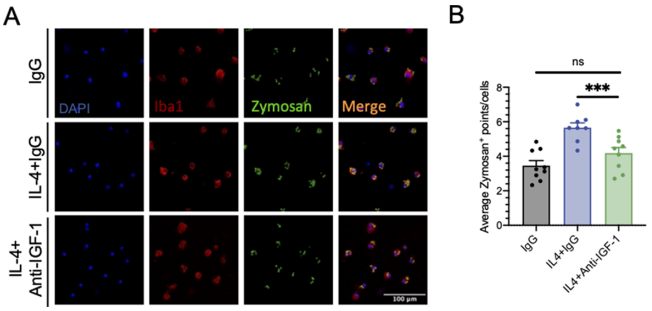

Figure 6. IGF-1 neutralizing antibody attenuates IL-4–induced M2-type microglial phagocytosis when CD11b is deleted. (**A**, **B**) Representative images and quantitative analysis showing immunofluorescent staining of Iba1 (*red*) and zymosan (*green*) with Hoechst (*blue*) nuclear staining in primary *Itgam*$^{-/-}$ microglia after IL-4 and IGF-1 neutralizing antibody or isotype control antibody treatment. Scale bar, 100 μm. The quantitative analysis illustrates that $IL\text{-}4^+$ isotype control antibody enhanced *Itgam*$^{-/-}$ microglial phagocytosis of zymosan particles; IGF-1 neutralizing antibody attenuates the phagocytosis-enhancing effect induced by $IL\text{-}4^+$ isotype control antibody. Each dot represents the average value of three to four visual fields in one culture (mean ± SEM, $n = 8$–9 wells per group).

Discussion

In TON, microglia are pivotal in the phagocytosis of debris, despite not having adequate clearance. The residual debris stimulates glia-mediated neuroinflammation,[41] causing secondary damage while impeding axonal regeneration. In this study, CD11b knockout led to increased microglia phagocytose of axonal debris after optic nerve injury in mice. Further experiments confirmed that this phenomenon may be due to enhanced secretion of microglia IGF-1 caused by CD11b knockout which in turn promotes the phagocytosis by M2-type microglia while decreasing axonal degradation and maintaining axonal integrity after ONC.

CD11b is a subunit of the integrin receptor complement receptor 3 and is involved in microglial phagocytosis.[42] Our results suggest that CD11b is involved in the phagocytic activity during ONC. Next, we investigated the role of CD11b in phagocytosis. It is noteworthy that the regulation of microglia phagocytosis in TON is complicated. Hematogenous macrophages also participate in the removal of cellular debris. Although we cannot exclude the possibility that macrophages also undertake the removal of axonal debris, the diffusion of macrophages is limited and mostly restricted to the core of the glial scar in ONC.[43] In the present study, we concluded that CD11b knockout enhanced the phagocytosis of axon debris by microglia around the crush site.

Microglia in different polarization states have different phagocytic behaviors.[44] We analyzed the polarization status of microglia in *Itgam*$^{-/-}$ mice. CD11b knockout caused a significant increase in IGF-1, although it failed to alter the polarization state of microglia. In the CNS, microglia are an

Investigative Ophthalmology & Visual Science

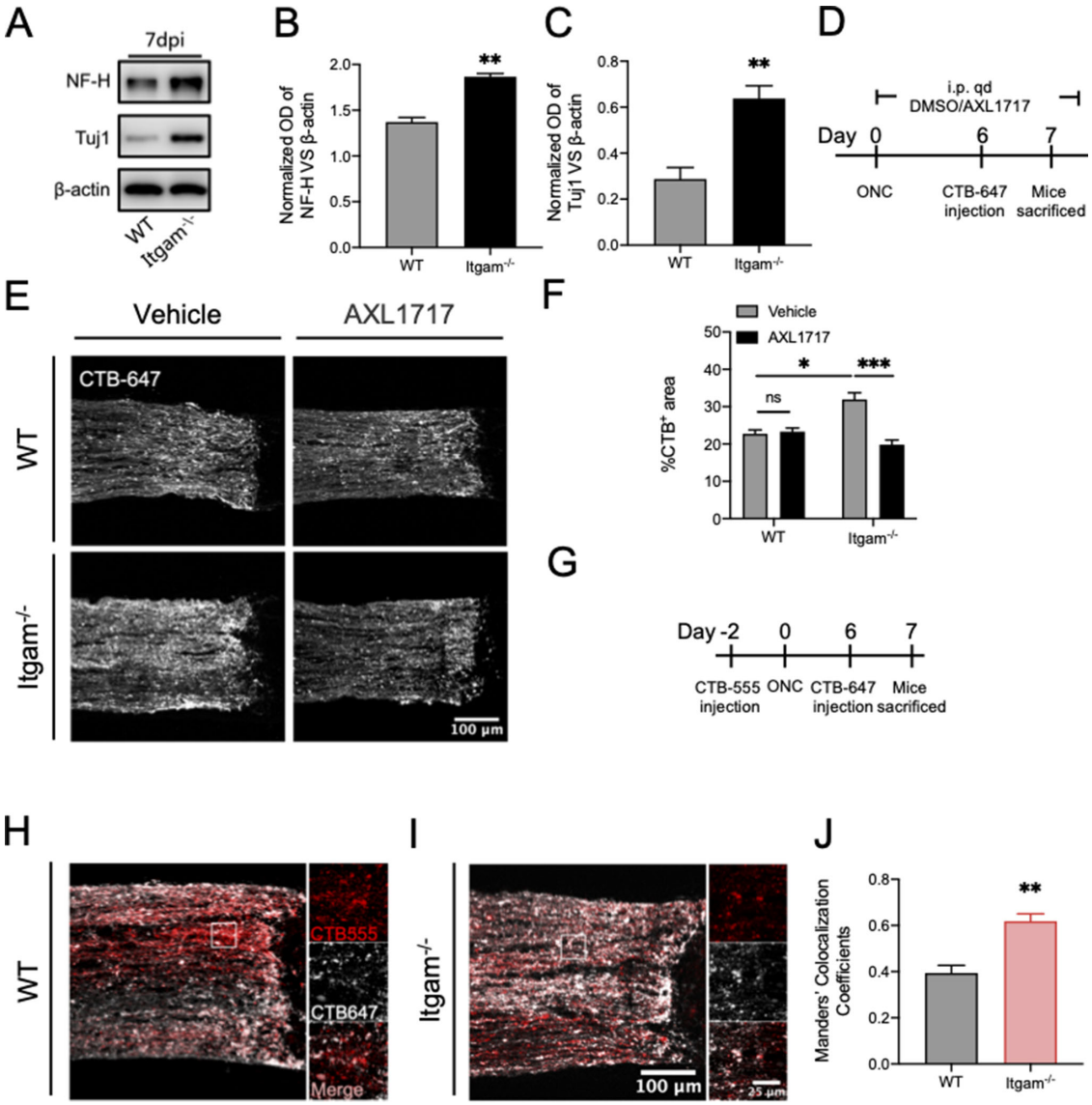

Figure 7. Reduced axonal degradation by CD11b/IGF-1 after ONC. (**A**) WB of NF-H and Tuj1 expression in the optic nerve at day 7 after ONC. β-Actin was used as a loading control. (**B**, **C**) Quantitative WB analysis indicates a significant upregulation of NF-H and Tuj1 (mean ± SEM, $n = 5$ mice per group). (**D**) Scheme of CTB labeling and optic nerve compression paradigm in (**E** and **F**). (**E**, **F**) Representative images and quantitative analysis of CTB^+ fields in the optic nerve proximal to the crush site at day 7 after injury. WT and *Itgam*$^{-/-}$ mice were administered DMSO (solvent) or AXL1717 intraperitoneally. Quantitative analysis shows the percentage of CTB $^+$ area to the tissue area ($n = 4$–5 mice per group). Error bars represent the mean ± SEM. Scale bar, 100 μm. (**G**) Scheme of CTB labeling and optic nerve compression paradigm in (**H**, **I**, and **J**). CTB-555 was used to pre-label retinal ganglion cell axons before surgery, followed by CTB-647 to label residual axons on day 6 after injury. Then mice were sacrificed on day 7. In this way, the $CTB555^+$ area colocalized with CTB-647 represents functional axons. In turn, the remaining $CTB555^+$ points were axonal debris that had not been or was being cleared. (**H**, **I**, and **J**) Representative images and quantitative analysis of CTB-555^+ fields (*red*) and CTB-647^+ fields (*white*) in the optic nerve proximal to the crush site at day 7 after injury. High-power images are from the white box area. Scale bar, 100 μm (enlarged, 25 μm). The quantitative analysis illustrates the ratio of the area of gray fluorescence colocalized with red fluorescence to the total area of red fluorescence within the tissue region. Fiji software is used to obtain the whole tissue region (the region of interest) in the visual field for colocalization analysis ($n = 3$ mice per group). Error bars represent mean ± SEM.

important source of IGF-1.[45] We found that the elevated IGF-1 in *Itgam*$^{-/-}$ mice was mainly derived from microglia. Our results identified a potential regulatory possibility of CD11b on the growth factor IGF-1, but the underlying mechanisms need to be explored further.

The effect of IGF-1 on phagocytosis has been reported.[34,46] Nevertheless, to our knowledge, the present study is the first to report the role of IGF-1 on M2-type microglia phagocytosis. We found that CD11b knockdown resulted in further elevation of IGF-1 secretion by M2 microglia. Elevated IGF-1 in turn promotes M2-type microglia phagocytosis. However, IGF-1 does not change the phagocytic ability of M1-type or resting-state (M0) microglia. The selectivity of IGF-1 phagocytosis regulation was also reported by Pinto-Benito et al.[34] Based on these results, we suggest that M2-type microglia may have a unique phagocytic pathway regulated by IGF-1.

Considering the neuroprotective effect of IGF-1,[47] we explored the effect of CD11b/IGF-1 on axonal degeneration after ONC. WB, immunohistochemical, and CTB label-

Investigative Ophthalmology & Visual Science

ing indicated *Itgam*$^{-/-}$ mice preserved more axons, and the IGF-1R inhibitor AXL1717 blocked this effect. Norris et al[10] also observed an increase in residual CTB^{+} area at the lateral geniculate nucleus in *Itgam*$^{-/-}$ mice after ONC. Similar to the above study, Peterson et al.[29] found that the myelin marker myelin basic protein was increased in *Itgam*$^{-/-}$ mice after optic nerve injury. Under the same degree of damage, the number of residual axonal or myelin markers in the optic nerve should be determined by a combination of both axonal and myelin disaggregation and axonal and myelin debris removal. We found that CD11b knockout resulted in an enhanced ability of microglia to phagocytose axonal debris (Figs. 3A, B, and C) and a decrease in axonal degradation after injury (Figs. 7E and F; Supplementary Fig. S5A and B). By sequentially labeling axons with CTB-555 and CTB-647 (Figs. 7H, I, and J), combined with the above results, we concluded that CD11b knockout could decrease axonal degradation after ONC by upregulating IGF-1.

In conclusion, this study is the first to report the involvement of CD11b in a novel phagocytosis regulatory pathway. In TON, CD11b knockout may promote microglia phagocytosis of axonal debris and reduce axonal degradation through IGF-1. Still, our study has some limitations. First, the mechanism of IGF-1 promoting phagocytosis in M2 microglia is not well-understood. Second, in our research, *Itgam*$^{-/-}$ mice showed several factors that promote regeneration, such as increased expression of IGF-1 and enhanced axonal debris clearance. Whether CD11b has a regulatory role in axonal regeneration remains to be investigated.

Acknowledgments

The authors especially thank Yuan-Guo Zhou and Feng Mei for project advice and data evaluation.

Supported by grants from the National Natural Science Foundation of China (No.82071392, No. 81870647) and Chongqing talent Outstanding scientist (2019).

Disclosure: **J. Zhou**, None; **S. Lin**, None; **Q. Hu**, None; **X. Li**, None; **X. Chen**, None; **L. Luo**, None; **S. Ye**, None; **W. Liu**, None; **J. Ye**, None

References

1. McKerracher L, David S, Jackson DL, Kottis V, Dunn RJ, Braun PE. Identification of myelin-associated glycoprotein as a major myelin-derived inhibitor of neurite growth. *Neuron*. 1994;13:805–811.
2. Vajda F, Jordi N, Dalkara D, et al. Cell type-specific Nogo-A gene ablation promotes axonal regeneration in the injured adult optic nerve. *Cell Death Differ*. 2015;22:323–335.
3. Ulland TK, Wang Y, Colonna M. Regulation of microglial survival and proliferation in health and diseases. *Semin Immunol*. 2015;27:410–415.
4. Colonna M, Butovsky O. Microglia function in the central nervous system during health and neurodegeneration. *Annu Rev Immunol*. 2017;35:441–468.
5. Au NPB, Ma CHE. Neuroinflammation, microglia and implications for retinal ganglion cell survival and axon regeneration in traumatic optic neuropathy. *Front Immunol*. 2022;13:860070.
6. Kopper TJ, Gensel JC. Myelin as an inflammatory mediator: Myelin interactions with complement, macrophages, and microglia in spinal cord injury. *J Neurosci Res*. 2018;96:969–977.
7. Lafuente EM, Niedergang F, Rosales C. Editorial: Phagocytosis: Molecular mechanisms and physiological implications. *Front Immunol*. 2020;11:586918.
8. Shi X, Luo L, Wang J, et al. Stroke subtype-dependent synapse elimination by reactive gliosis in mice. *Nat Commun*. 2021;12:6943.
9. Anderson AJ, Robert S, Huang W, Young W, Cotman CW. Activation of complement pathways after contusion-induced spinal cord injury. *J Neurotrauma*. 2004;21:1831–1846.
10. Norris GT, Smirnov I, Filiano AJ, et al. Neuronal integrity and complement control synaptic material clearance by microglia after CNS injury. *J Exp Med*. 2018;215:1789–1801.
11. Cai XF, Lin S, Geng Z, et al. Integrin CD11b deficiency aggravates retinal microglial activation and RGCs degeneration after acute optic nerve injury. *Neurochem Res*. 2020;45:1072–1085.
12. Szklarczyk D, Gable AL, Nastou KC, et al. The STRING database in 2021: Customizable protein-protein networks, and functional characterization of user-uploaded gene/measurement sets. *Nucleic Acids Res*. 2021;49:D605–D612.
13. Qu J, Jakobs TC. The time course of gene expression during reactive gliosis in the optic nerve. *PloS One*. 2013;8:e67094.
14. Edgar R, Domrachev M, Lash AE. Gene Expression Omnibus: NCBI gene expression and hybridization array data repository. *Nucleic Acids Res*. 2002;30:207–210.
15. Davis S, Meltzer PS. GEOquery: A bridge between the Gene Expression Omnibus (GEO) and BioConductor. *Bioinformatics*. 2007;23:1846–1847.
16. Bardou P, Mariette J, Escudie F, Djemiel C, Klopp C. jvenn: An interactive Venn diagram viewer. *BMC Bioinform*. 2014;15:293.
17. Ashburner M, Ball CA, Blake JA, et al. Gene ontology: Tool for the unification of biology. The Gene Ontology Consortium. *Nat Genet*. 2000;25:25–29.
18. Palasca O, Santos A, Stolte C, Gorodkin J, Jensen LJ. TISSUES 2.0: An integrative web resource on mammalian tissue expression. *Database (Oxford)*. 2018;2018:1–12.
19. Wickham H. *ggplot2: Elegant graphics for data analysis. Use R!* 2nd ed. Cham, Germany: Springer International Publishing; 2016:1–260.
20. Zhou JX, Liu YJ, Chen X, et al. Low-intensity pulsed ultrasound protects retinal ganglion cell from optic nerve injury induced apoptosis via Yes associated protein. *Front Cell Neurosci*. 2018;12:160.
21. Yun-Jia L, Xi C, Jie-Qiong Z, Jing-Yi Z, Sen L, Jian Y. Semaphorin3A increases M1-like microglia and retinal ganglion cell apoptosis after optic nerve injury. *Cell Biosci*. 2021;11:97.
22. Sidman RL, Li J, Lawrence M, et al. The peptidomimetic Vasotide targets two retinal VEGF receptors and reduces pathological angiogenesis in murine and nonhuman primate models of retinal disease. *Sci Transl Med*. 2015;7:309ra165.
23. Giulian D, Baker TJ. Characterization of ameboid microglia isolated from developing mammalian brain. *J Neurosci*. 1986;6:2163–2178.
24. Czirr E, Castello NA, Mosher KI, et al. Microglial complement receptor 3 regulates brain Abeta levels through secreted proteolytic activity. *J Exp Med*. 2017;214:1081–1092.
25. Molnar K, Meszaros A, Fazakas C, et al. Pericyte-secreted IGF2 promotes breast cancer brain metastasis formation. *Mol Oncol*. 2020;14:2040–2057.
26. Zhu H, Sun X. Three-dimensional structure of axonal mitochondria reflects the age of drosophila. *Neural Regen Res*. 2013;8:616–621.

27. Di Tomaso MV, Vazquez Alberdi L, Olsson D, et al. Colocalization analysis of peripheral myelin protein-22 and lamin-B1 in the Schwann cell nuclei of Wt and TrJ mice. *Biomolecules*. 2022;12:1–23.
28. Bosch M. Introduction to ImageJ macro language in a particle counting analysis: Automation matters. *Methods Mol Biol*. 2019;2040:51–70.
29. Peterson SL, Li Y, Sun CJ, et al. Retinal ganglion cell axon regeneration requires complement and myeloid cell activity within the optic nerve. *J Neurosci*. 2021;41:8508–8531.
30. Wen RX, Shen H, Huang SX, et al. P2Y6 receptor inhibition aggravates ischemic brain injury by reducing microglial phagocytosis. *CNS Neurosci Ther*. 2020;26:416–429.
31. Dong B, Pang TT. LncRNA H19 contributes to Rh2-mediated MC3T3-E1cell proliferation by regulation of osteopontin. *Cell Mol Biol (Noisy-le-grand)*. 2017;63:1–6.
32. Wang C, Yue H, Hu Z, et al. Microglia mediate forgetting via complement-dependent synaptic elimination. *Science*. 2020;367:688–694.
33. He J, Mu M, Wang H, et al. Upregulated IGF1 in the lungs of asthmatic mice originates from alveolar macrophages. *Mol Med Rep*. 2019;19:1266–1271.
34. Pinto-Benito D, Paradela-Leal C, Ganchala D, de Castro-Molina P, Arevalo MA. IGF-1 regulates astrocytic phagocytosis and inflammation through the p110alpha isoform of PI3K in a sex-specific manner. *Glia*. 2022;70:1153–1169.
35. Orihuela R, McPherson CA, Harry GJ. Microglial M1/M2 polarization and metabolic states. *Br J Pharmacol*. 2016;173:649–665.
36. Li L, Gan H, Jin H, et al. Astragaloside IV promotes microglia/macrophages M2 polarization and enhances neurogenesis and angiogenesis through PPARgamma pathway after cerebral ischemia/reperfusion injury in rats. *Int Immunopharmacol*. 2021;92:107335.
37. Allendorf DH, Puigdellivol M, Brown GC. Activated microglia desialylate their surface, stimulating complement receptor 3-mediated phagocytosis of neurons. *Glia*. 2020;68:989–998.
38. Labandeira-Garcia JL, Costa-Besada MA, Labandeira CM, Villar-Cheda B, Rodriguez-Perez AI. Insulin-like growth factor-1 and neuroinflammation. *Front Aging Neurosci*. 2017;9:365.
39. Rauskolb S, Dombert B, Sendtner M. Insulin-like growth factor 1 in diabetic neuropathy and amyotrophic lateral sclerosis. *Neurobiol Dis*. 2017;97:103–113.
40. Nuschke AC, Farrell SR, Levesque JM, Chauhan BC. Assessment of retinal ganglion cell damage in glaucomatous optic neuropathy: Axon transport, injury and soma loss. *Exp Eye Res*. 2015;141:111–124.
41. Joshi AU, Minhas PS, Liddelow SA, et al. Fragmented mitochondria released from microglia trigger A1 astrocytic response and propagate inflammatory neurodegeneration. *Nat Neurosci*. 2019;22:1635–1648.
42. Bednarczyk M, Stege H, Grabbe S, Bros M. beta2 integrins-multi-functional leukocyte receptors in health and disease. *Int J Mol Sci*. 2020;21:1–43.
43. Jin H, Liu Y, Liu X, Khodeiry MM, Lee JK, Lee RK. Hematogenous macrophages contribute to fibrotic scar formation after optic nerve crush. *Mol Neurobiol*. 2022;59:7393–7403.
44. Wang J, Xing H, Wan L, Jiang X, Wang C, Wu Y. Treatment targets for M2 microglia polarization in ischemic stroke. *Biomed Pharmacother*. 2018;105:518–525.
45. Suh HS, Zhao ML, Derico L, Choi N, Lee SC. Insulin-like growth factor 1 and 2 (IGF1, IGF2) expression in human microglia: Differential regulation by inflammatory mediators. *J Neuroinflammation*. 2013;10:37.
46. Mu M, Wu F, He J, et al. Insulinlike growth factor 1 inhibits phagocytosis of alveolar epithelial cells in asthmatic mice. *Mol Med Rep*. 2019;20:2381–2388.
47. Bhalla S, Mehan S, Khan A, Rehman MU. Protective role of IGF-1 and GLP-1 signaling activation in neurological dysfunctions. *Neurosci Biobehav Rev*. 2022;142:104896.

Investigative Ophthalmology & Visual Science